

# **STUDY OF THE PHOTOCATALYTIC DEGRADABILITY OF CERAMIC GLAZES**

**O.Ruiz<sup>(1)</sup>, F. Sanmiguel<sup>(1)</sup>, C. Gargori<sup>(2)</sup>, F.Galindo<sup>(2)</sup>, G. Monrós<sup>(2)</sup>**

<sup>(1)</sup> TORRECID S.A. Alcora (Spain)

<sup>(2)</sup> Department of Inorganic and Organic Chemistry, Universidad Jaime I,  
Castellón (Spain)

## 1. INTRODUCTION

The purpose of any wastewater treatment process is to eliminate the pollutants present in an effluent, so that after treatment, this conforms to the legal specifications in regard to discharge <sup>[1]</sup>. The processes and technologies available at the moment for the treatment of water pollutants are quite varied and may be divided in the following general groups:

- **Natural treatments:** These are based on the use of natural reagents. They involve techniques like the Green Filter or Pond Filter. They are usually not widely used given their low effectiveness.
- **Primary treatments:** These are processes in which the suspended particles present in the water to be treated are separated by physical means. The methods include Decantation, Homogenisation, Sieving or Filtering, Coagulation–Flocculation, Precipitation, and Neutralisation.
- **Secondary treatments:** These essentially consist of biological processes that degrade the biodegradable organic matter. Secondary treatments are grouped into two large groups: aerobic and anaerobic processes. They are relatively cheap but are not very ineffective with toxic pollutants (such as pesticides).
- **Tertiary treatments:** Tertiary treatments have been traditionally considered refining processes for the removal of pollutants that could not be removed in the foregoing treatment phases. They usually include processes like Adsorption, Ion Exchange, Ultrafiltration, Membrane Processes, Electrodialysis, Stripping, Disinfection, Conventional Oxidation Processes, and also so-called Advanced Oxidation Processes (AOPs).

At the present time tertiary treatments tend to be increasingly used, in order to conform to (increasingly demanding) regulations on water quality and to achieve more effective recycling. In tertiary treatments, AOPs constitute one of the most advanced techniques in the treatment of water polluted with organic products. The advantage of this technique, as opposed to others, is based on the possibility of eliminating organic products, such as pesticides, organic and biocide colorants, which cannot be treated by other conventional techniques due to their high chemical stability and low biodegradability <sup>[2-5]</sup>.

Advanced oxidation processes are tertiary treatment processes based on the generation of strongly oxidising species. Among the AOPs, those that produce the hydroxyl radical ( $\bullet\text{OH}$ ) are the most successful, because this species is strongly oxidising (oxidation potential 2.8eV). Since these radicals are very vigorous oxidising agents, they are able to decompose organic compounds and make them harmless. These radicals are generated by a photocatalytic processes.

Photocatalysis is a catalytic process that produces a photochemical alteration of certain chemical species as a result of radiation absorption by another photosensitive species (catalyst). Two types of photocatalysis are differentiated, based on the catalyst:

- **Homogeneous photocatalysis:** In this case the catalyst (usually iron) is dissolved in the water containing the pollutants to be treated, which is why all the elements that take part in the process are in the same phase. The most widely known homogeneous photocatalytic process is the photo-Fenton, based on the use of the Fenton reagent (described by H. J. H. Fenton at the end

of the 19<sup>th</sup> century) [6]. The Fenton reagent or method is a mixture of iron(II) salts and hydrogen peroxide, which produces the hydroxyl radical as an active species, according to the following reaction:



In the photo-Fenton process sunlight or UV light is used, which allows additional  $\text{OH}\cdot$  radicals to be obtained and regenerates the  $\text{Fe}^{2+}$  ion, which act as a homogeneous catalyst, in accordance with the reaction:



- Heterogeneous photocatalysis:** In heterogeneous photocatalysis, a semiconductor solid is used ( $\text{TiO}_2$ ,  $\text{ZnO}$ ,  $\text{ZrO}_2$ ,  $\text{CeO}_2$ ,  $\text{CdS}$ ,  $\text{ZnS}$ , etc.) that forms a dispersion under irradiation to stimulate a reaction in the solid-liquid or solid-gas interface. The photoreaction mechanism begins when the semiconductor is irradiated with photons whose energy is equal to or larger than the existing energy gap between the valence and the conduction band ( $E_g$ ). In this situation, those photons are absorbed and electron-hole pairs are created in the catalyst, which dissociate into free photoelectrons in the conduction band and photo-holes in the valence band. Concurrently, the pollutants are adsorbed and the photo-hole generates a radical hydroxyl ( $\text{OH}\cdot$ ) that will oxidise the adsorbed pollutant. The net electron flow is zero and the catalyst remains unaltered, as shown in the scheme in Figure 1.

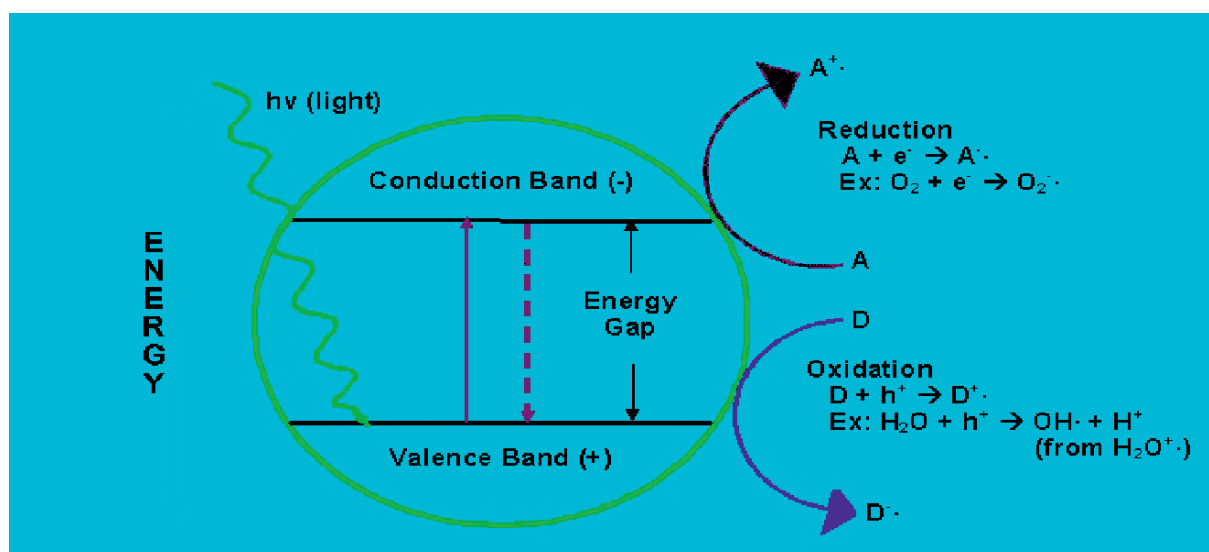
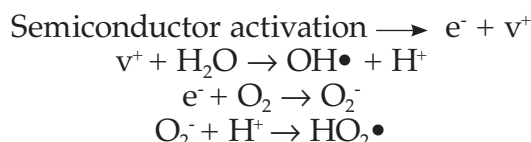


Figure 1. Schematic illustration of a heterogeneous photocatalysis process

From a spectroscopic viewpoint, semiconductor species are characterised by displaying a single broad absorption band in the violet-blue region, associated with the charge transfer from the valence band to the conduction band. The frequency threshold  $\nu$  beyond which absorption is effective determines the band energy gap  $E_g$ , in which  $E_g = h\nu$  where  $h$  is Planck's constant ( $6,624 \cdot 10^{-34}$  Js). The  $E_g$  values of most semiconductors involve the use of light in the ultraviolet region during the photocatalytic treatment processes.

Effective photocatalytic degradation processes should produce the complete mineralisation of the degraded substrates; however, the process often ends in intermediate compounds if these exhibit no toxicity or there are no exposure risks.

In general, photocatalytic degradation follows the Langmuir-Hinshelwood model [7-9]. In heterogeneous catalysis processes the Langmuir-Hinshelwood model considers the reaction between two species adsorbed on the catalyst (adsorbates). The foundation of this model is a unimolecular reaction that may be represented according to the following equilibrium:



The limiting or determining step of the mechanism is the decomposition step at the catalyst surface, so that the reaction rate considered pseudo-first order is the product of the kinetic constant associated with the decomposition by the adsorbate concentration  $\Theta_A$  given by the Langmuir adsorption equation

$$(1) \quad \Theta_A = \frac{Kc}{1 + Kc}$$

In short, the substrate elimination or degradation rate  $r$  is given by the following equation:

$$(2) \quad r = \frac{dc}{dt} = k \left[ \frac{Kc}{1 + Kc} \right]$$

where  $k$  is the rate constant dependent on luminous intensity,  $K$  is the adsorption constant, and  $c$  is the substrate concentration it is intended to degrade.

At low adsorption and also at low concentration ( $Kc \ll 1$ ), Equation (2) turns out to be a pseudo-first-order kinetics:

$$(3) \quad r = kKc$$

separating variables:

$$(4) \quad \frac{dc}{dt} = kKc \Rightarrow \frac{dc}{c} = kKdt$$

and integrating between the initial conditions  $t=0$ ,  $c=c_0$  and at a time  $t$  gives the integrated equation (5).

$$(5) \quad \ln \frac{c}{c_0} = kKt$$

If we define the half-life period  $t_{1/2}$  as the time needed to reduce, under these conditions, the substrate concentration by half, Equation (5) becomes:

$$(6) \quad \ln \frac{c_0/2}{c_0} = kKt_{1/2}$$

Yielding:

$$(7) \quad t_{1/2} = -\frac{\ln 2}{kK}$$

If, in contrast, the adsorption is high and/or the concentration is high ( $Kc \gg 1$ ), Equation (2) is reduced to a zero-order kinetics and therefore, adsorption dominates the process:

$$r = k \quad (7)$$

In this sense it may be stated that the reaction rate displays a dependence on the concentration according to Figure 2 which shows a pseudo-first-order kinetics at low concentrations and a zero-order kinetics at high concentrations.

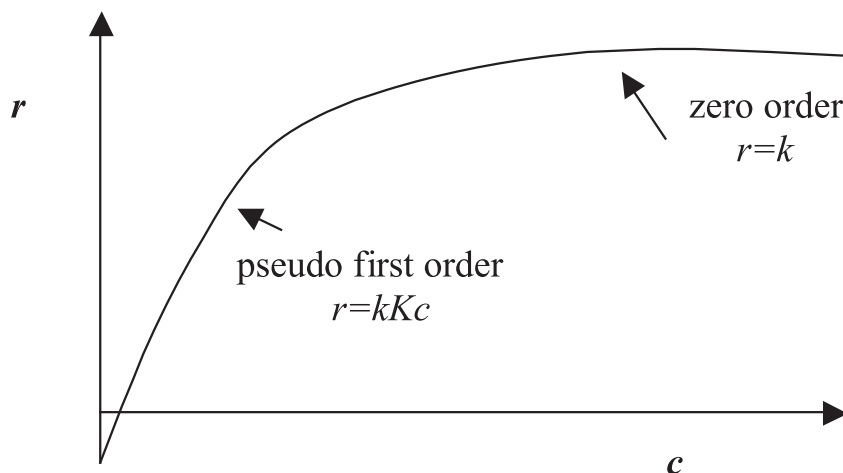


Figure 2. Evolution of kinetics in the Langmuir-Hinshelwood mechanism.

Photodegradation studies are conducted with different species that exhibit absorption at a particular wavelength  $\lambda$ . The variation in absorption allows the degradation of the indicator to be studied and, therefore, the photocatalytic process, experimentally determining the mentioned half-life period ( $t_{1/2}$ ). Among others, the Orange II acid, a sulphonated monoazo colorant of molecular formula  $C_{16}H_{11}N_2SO_4Na$ , is used as model colorant in photocatalytic degradation studies.

## 2. OBJECTIVE

Anatase is the semiconductor used as a heterogeneous photocatalytic agent in discharge treatment, there being a wide variety of Anatase-based powders in the photocatalytic market. The photodegradation process is based on the formation of a suspension of Anatase in the wastewater to be treated. After a residence time the photocatalyst is removed by decantation and the water is filtered, which requires working in a discontinuous operating regime, and leads to high processing costs.

The present work seeks to evaluate the possibility of using different types of ceramic glazes consisting of different crystalline phases as alternatives to the use of Anatase powder in photocatalytic treatment and cleaning processes. This was done using the Orange II indicator as a tracer in the study of the catalytic photodegradation process.

### 3. EXPERIMENTAL

#### 3.1. MATERIALS

Commercial Anatase P25 supplied by Degussa was used as a reference material with which to compare the photocatalytic behaviour of the different glazes.

In regard to the glazes, three approaches were used to obtain the different crystalline phases. On the one hand, glazes were developed that contained different frits which devitrified the desired phases. Glaze suspensions were therefore prepared and applied on to a previously engobed body. They were then fired by a standard wall tile firing cycle.

In order to study the influence of the devitrified zircon phase content on photocatalytic activity, mixtures were prepared with different quantities of a standard transparent frit and a frit with a 12.5%  $ZrO_2$  content. The frit mixtures were milled together and the different glaze suspensions were prepared using the additives customarily employed in ceramic glaze manufacture. The glazes were then applied on to a body that had been previously coated with a standard wall tile engobe, after which the ensemble was fired according to a standard wall tile firing cycle.

Finally, the third approach consisted of the development of layers of lustre with different  $TiO_2$  contents on an already fired glazed body. For this, different screen printing compositions consisting of the mixture of a Ti alkoxide, together with the necessary additives for appropriate application, were prepared. Once the screen print had been applied, it was subjected to a firing cycle with a peak temperature of 790°C.

#### 3.2. CHARACTERISATION TECHNIQUES

The photocatalytic activity of the different glazes was characterised using the monoazo Orange II colorant. The concentration of the solution used was  $0.6 \cdot 10^{-4}$  M buffered at pH 7.4 ( $NaH_2PO_4 \cdot H_2O$  3.31 g and  $Na_2HPO_4 \cdot 7H_2O$  33.77 g made up to 1 L).

Based on the spectrum of the Orange II solution, 485nm was established as the measurement wavelength for the colorimetric monitoring.

Irradiation was conducted with a 125W medium pressure Mercury lamp. The emission spectrum displayed three characteristic lines at 254nm, 313nm, and 365 nm.

The photocatalytic characterisation was carried out of the commercial Anatase powder as well as of the different glazes obtained. A 1 litre solution of Orange II was prepared in all cases according to the concentrations indicated previously. This solution was placed in a container that held the Mercury lamp, as shown in Figure 3. In the case of the Anatase powder, the measurement procedure of the photocatalytic activity consisted of studying the degradation of 1 litre Orange II solution containing a suspension of 0.5g Anatase, and measuring the variation in the band at 485nm at set periods of time. The glazes were characterised by placing six pieces measuring 14x4cm in the reactor together with the Orange II solution. Just as with the Anatase, an aliquot was taken at set times and the variation in the band at 485nm was measured. Finally, in all cases, a graph was constructed in which time was plotted versus absorbance at 485 nm. This graph thus showed the evolution of Orange II degradation and the half-life period obtained in each case.



Figure 3. Photocatalytic degradation cell.

Since every photocatalytic process has an associated photolysis phenomenon (non-catalysed degradation), a blank test was also conducted without the presence of the photocatalyst powder or the ceramic tiles with a view to determining the time after which the degradation corresponded to a photolysis phenomenon, and there was no photocatalysis.

In addition to the study and the photocatalytic characterisation, other materials characterisation techniques were also used.

Since photoactivity is a surface phenomenon, the glazed surfaces were characterised by grazing incidence X-ray diffraction or XRD with a low angle of incidence. The use of this specific diffraction technique is justified by the limitation of conventional diffractometers for the study of thin layers since the X-rays penetrate much farther into the sample than the layer thickness and underlying crystals are detected that play no part in the photocatalytic process.

If the sample surface is exposed to low-angle radiation (typically  $\leq 2^\circ\Theta$ ), the effective length of the beam increases an order of magnitude when it crosses the surface. In the surface incidence device, the conventional Bragg-Brentano X-ray focalisation is converted into a parallel decoupled beam by mounting an accessory with a Soller slit in which the sheets are arranged at right angles to the diffraction plane<sup>[10]</sup>. In this study, carried out in a Siemens D5000 diffractometer, a low divergence slit ( $0.1^\circ$ ), a Soller slit to limit the axial divergence on the tube side, and long slits on the detector side (divergences of  $0.2^\circ\Theta$  or  $0.4^\circ\Theta$ ) have been used.

UV-V-NIR spectroscopy of the glazed surfaces was conducted in a Perkin Elmer Lambda 2000 spectrophotometer by the diffuse reflectance method. The spectra of semiconducting materials like the ones being studied display a charge transfer band in the UV-V frequency range that shifts to lower wavelengths (higher energies) when

the particles of the material are nanometre size. The band energy of the semiconductor, needed for its conductivity, is measured from the absorption frequency threshold in the spectrum.

The SEM-EDX (scanning electron microscopy and coupled energy-dispersive X-ray analysis) studies were conducted to analyse the surface of the deposited material and surface chemical composition.

The gloss of the different glazes was measured with a Minolta model 268 glossmeter, using the conventional method of photometric comparison with a standard glass at different angles of incidence.

With a view to measuring the degree of roughness of the surface, the conventional method with the pick-up of a roughness meter (SM-3 from Kosaka Laboratory Ltd.) was used, which provides the average of the deviations with respect to the baseline  $R_a$  (average roughness) in a travel of 5-10 cm by the pick-up across the surface. The differential interferometry method was used to analyse the micrometric roughness by optical reflection measurements of the same beam on the test surface and on a standard surface, the difference between both reflections being proportional to the local topography of the notch area (of the order of 0.1x0.1 mm).

## 4. RESULTS

### 4.1. PHOTOCATALYTIC CHARACTERISATION OF THE COMMERCIAL ANATASE AND THE BASE GLAZE

Before the start of the photocatalytic study of the different glazes, the photocatalytic activity of the Anatase and transparent base glaze was characterised, as well as the photolytic degradation value of the blank, i.e. the degradation time when the reactor only contained Orange II without Anatase or wall tiles.

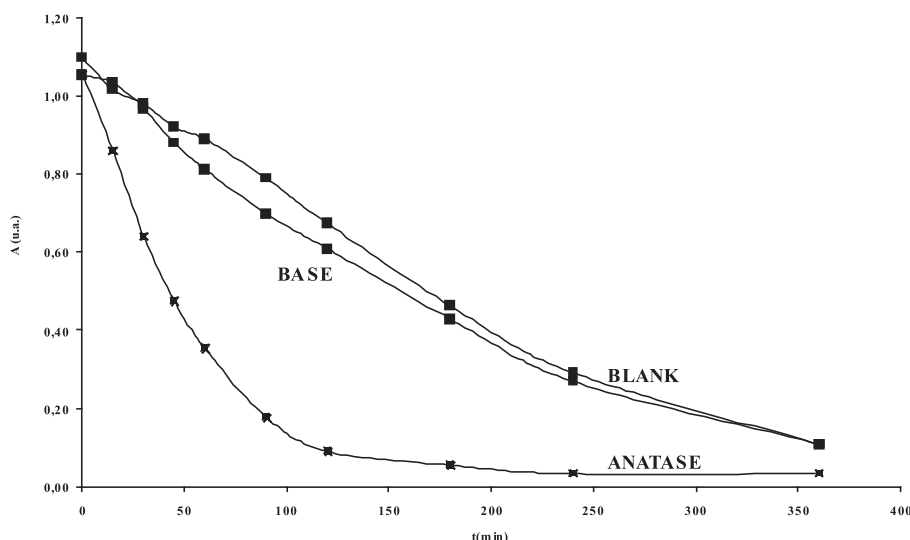


Figure 4. Evolution of the photocatalytic activity of the blank, base glaze, and commercial Anatase with time.

Figure 4 shows the evolution of the photocatalytic activity of the blank, the commercial Anatase, and the transparent base glaze. From these graphs, and following the Langmuir-Hinshelwood model, a half-life period ( $t_{1/2}$ ) was obtained of 42.6 minutes for the Anatase, 130 minutes for the transparent base glaze, and 151 minutes for the blank. In regard to the gap energy obtained from the UV-V spectrum, the Anatase displayed an  $E_g$  of 3.23 eV.

#### 4.2. EFFECT OF THE DEVITRIFIED PHASE ON THE PHOTOCHEMICAL CAPACITY

As indicated in section 3.1, the photocatalytic capacity of glazes that devitrified different types of crystalline phases was studied.

All glazes were characterised by grazing incidence X-ray diffraction with a view to determining the devitrified crystalline phases in each case. The detected phases are given in Table 1.

GLAZE	DEVITRIFIED PHASE	CHEMICAL FORMULA
1	Titanite	$\text{CaTiO}(\text{SiO}_4)$
2	Celsian	$\text{BaAl}_2(\text{SiO}_4)_2$
3	Diópside	$\text{CaMg}(\text{SiO}_3)_2$
4	Diópside + Anorthite	$\text{CaMg}(\text{SiO}_3)_2 + \text{CaAl}(\text{SiO}_4)_2$
5	Anorthite	$\text{CaAl}(\text{SiO}_4)_2$
6	Zircón	$\text{ZrSiO}_4$
7	Cassiterite	$\text{SnO}_2$
8	Gahnite	$\text{ZnAl}_2\text{O}_4$
9	Spodumene	$\text{LiAlSi}_2\text{O}_6$
10	Sheelite	$\text{CaWO}_4$

Table 1. Devitrified crystalline phases.

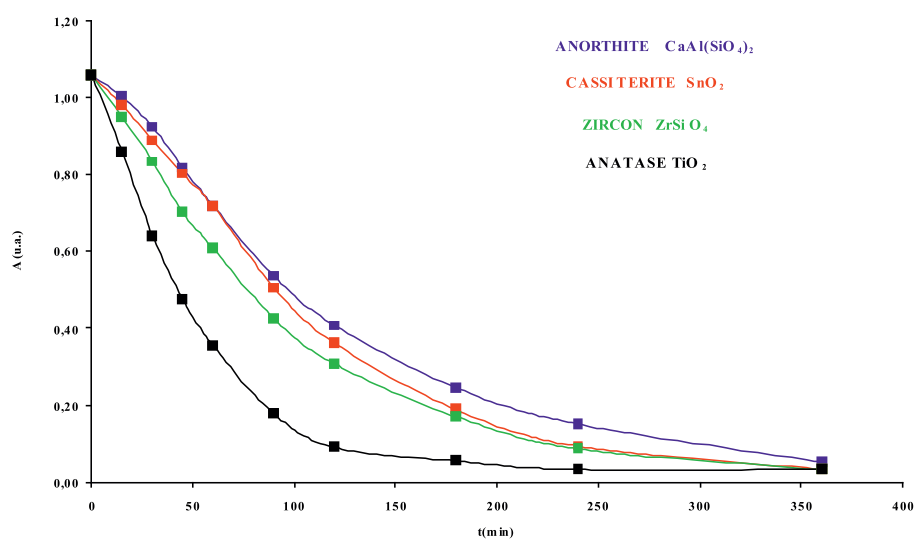


Figure 5. Evolution of the photocatalytic activity of commercial Anatase and of glazes in which Anorthite, Cassiterite, and Zircon devitrify.

In the study of photocatalytic degradation, the degradability of Orange II was only detected in glazes 5, 6, and 7, which devitrified Anorthite, Zircon, and Cassiterite, respectively. The photocatalysis plots of these three crystalline phases with photocatalytic activity, as well as the plot corresponding to the commercial Anatase, are shown in Figure 5.

The best results were observed in the sample that devitrified Zircon, since it improved the photocatalytic activity of the base glaze by 33%. The glaze that devitrified Cassiterite and Anorthite exhibited smaller improvements, of the order of 12%. The remaining devitrified samples displayed kinetics with activity resembling or worse than the base glaze. The Titanite crystalline phase should be noted because even though Anatase was added to the base glaze, the crystalline phase that developed was not Anatase or its allotrope Rutile but titanite oxosilicate with a low photocatalytic capacity despite this being a Titanium-based structure. This result evidences the importance of the semiconducting phase in the photocatalytic properties of the glazes.

Figure 6 presents the UV-V spectra of the phases that showed photocatalytic activity and the glaze that devitrified Titanite. These spectra allowed calculation of the band gap energy of each crystalline phase (Table 2). The  $E_g$  calculations seem to indicate that values exceeding 3.7eV with absorption thresholds of the order of 300nm display no photocatalytic capacity under the experimental working conditions.

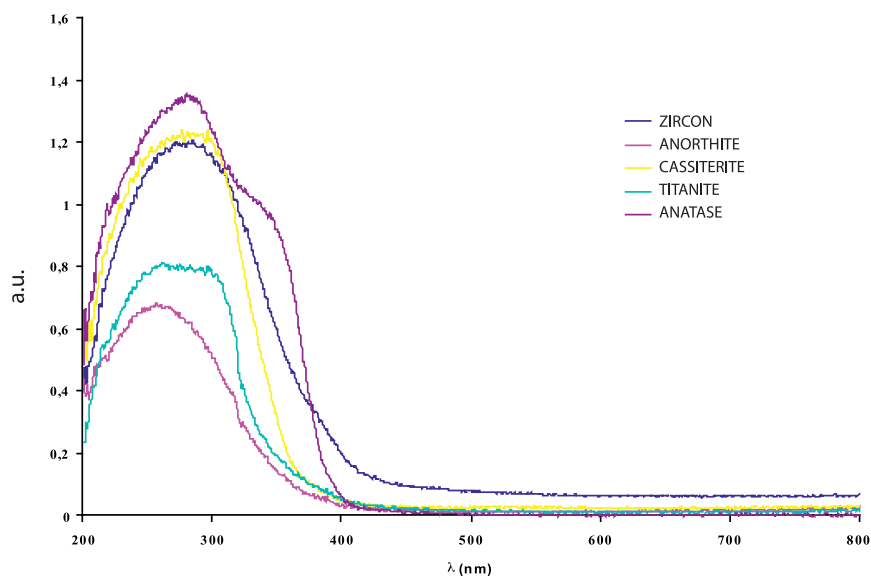


Figure 6. U.V-V spectra of commercial Anatase and glazes with the crystalline phases Zircon, Anorthite, Cassiterite, and Titanite.

	$E_g$ (eV)	$t_{1/2}$ (min)
Anatase	3,23	42,6
Anorthite	3,60	120,4
Cassiterite	3,50	112,0
Zircon	3,65	87,3
Titanite	3,81	148,0

Table 2. Kinetic data of the devitrified samples

#### 4.3. EFFECT OF THE ZIRCON PHASE FRACTION ON PHOTOCATALYTIC DEGRADABILITY

Since the zircon phase displayed the best photocatalytic degradation results, it was decided to study the influence of the devitrified Zircon phase content on the photocatalytic degradability of Orange II.

The study of the photocatalytic capacity was carried out using a frit with a  $ZrO_2$  content of 12.5%. By mixing this frit with another transparent one that generated no crystallisations, glazes with different Zircon contents were obtained that ranged from 2.5% to 12.5%, expressed as  $ZrO_2$ . Each of the mixtures was applied as a glaze according to the usual techniques for the obtainment of porous single-fire glazes. They were then subjected to firing by a standard cycle. Finally they were characterised from a crystallographic (XRD), spectroscopic (UV-V), and photocatalytic (degradation test with Orange II) viewpoint.

Figure 7 shows the diffraction spectra of the different glazes. It may be observed that starting at 4.5%  $ZrO_2$ , the  $ZrSiO_4$  peak that has devitrified in the frit during heat treatment can be clearly detected.

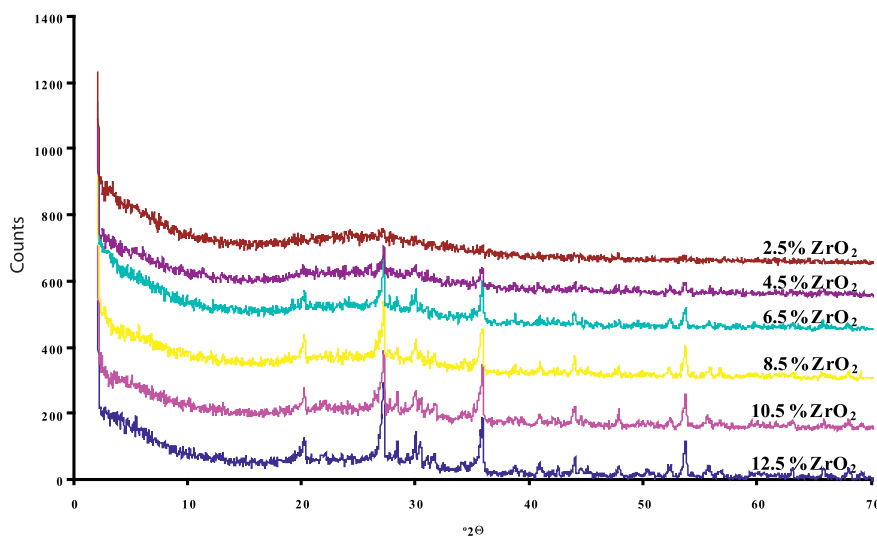


Figure 7. Grazing incidence X-ray diffraction of glazes that devitrify  $ZrSiO_4$  from different  $ZrO_2$  contents before firing.

The UV-V spectra were also obtained with a view to calculating the band gap energy of each composition, which are shown in Figure 8. An  $E_g$  value of 3.65 eV was obtained in all compositions.

Finally, to complete the study of the different glazes that devitrified Zircon, a study was conducted of photocatalytic degradation. Figure 9 shows the different photocatalytic degradation curves of the compositions, as well as the one corresponding to the Anatase powder. It may be observed in the graph that none of the compositions exhibited a photochemical activity close to that of Anatase, though those with a larger  $ZrO_2$  content in the frit developed shorter half-life periods than the compositions with a smaller  $ZrO_2$  content.

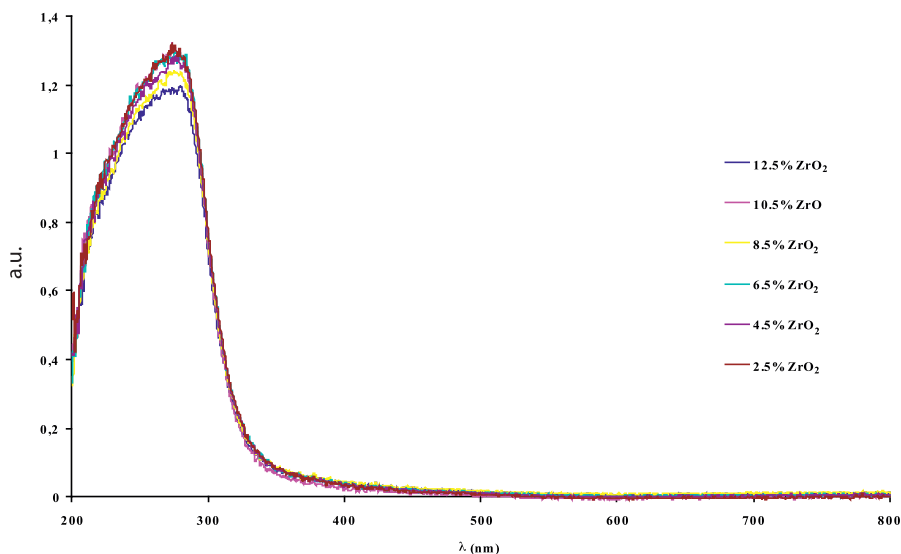


Figure 8. UV-V spectra of the different glazes that devitrify  $ZrSiO_4$  from different  $ZrO_2$  contents before firing.

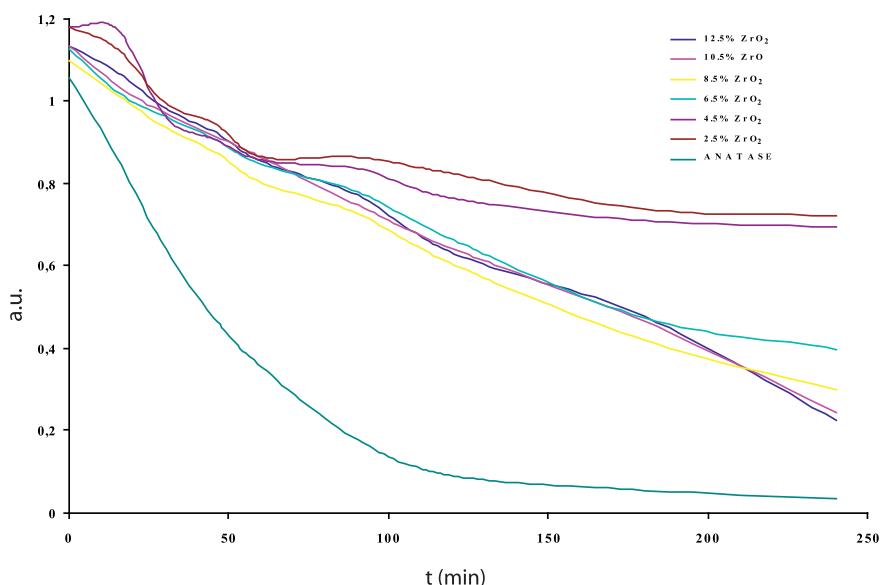


Figure 9. Evolution of the photocatalytic activity of commercial Anatase and of the glazes that devitrify  $ZrSiO_4$  from different  $ZrO_2$  contents before firing.

Table 3 gives the half-life periods obtained for each composition:

$\%ZrO_2$	2.5	4.5	6.5	8.5	10.5	12.5
$t_{1/2}(\text{min})$	94.5	83.1	82.0	78.7	75.8	74.2

Table 3. Values of  $t_{1/2}$  as a function of the  $ZrO_2$  % in the frit.

The  $E_g$  values and half-life periods indicate that, though the band gap energy is 3.65eV in all cases, the half-life periods increase when the  $ZrO_2$  content in the frit decreases, so that it may be stated that though the band gap value indicates the semiconducting character of the compound, it does not exclusively determine subsequent photochemical degradability. On the other hand the values of the half-

life period decrease as the  $ZrO_2$  content in the frit increases, which demonstrates the existence of a certain photocatalytic capacity in the glazes with  $ZrSiO_4$ .

The decrease in the half-life period at constant band gap energy indicates the existence of other variables that also influence photochemical degradability. A study of the evolution of the devitrification of the glazes by scanning electron microscopy, as well as of the gloss and roughness, has provided the results given in Table 4.

%ZrO <sub>2</sub>	2.5	4.5	6.5	8.5	10.5	12.5
Ra(μm)	0.10	0.07	0.14	0.43	1.17	1.05
Gloss 60°	94.8	94.4	92.2	74.3	59.2	11.2

Table 4. Roughness and gloss values

Figure 10 shows that the evolution of glaze surface microstructure with the increase in the  $ZrO_2$  concentration in the samples reveals the appearance of acicular Zirconium silicate crystal shapes that decrease in size with increased concentration (acicular crystal length is 2μm in the sample with 2.5%  $ZrO_2$  and this decreases progressively to 0.8μm in the more concentrated sample).

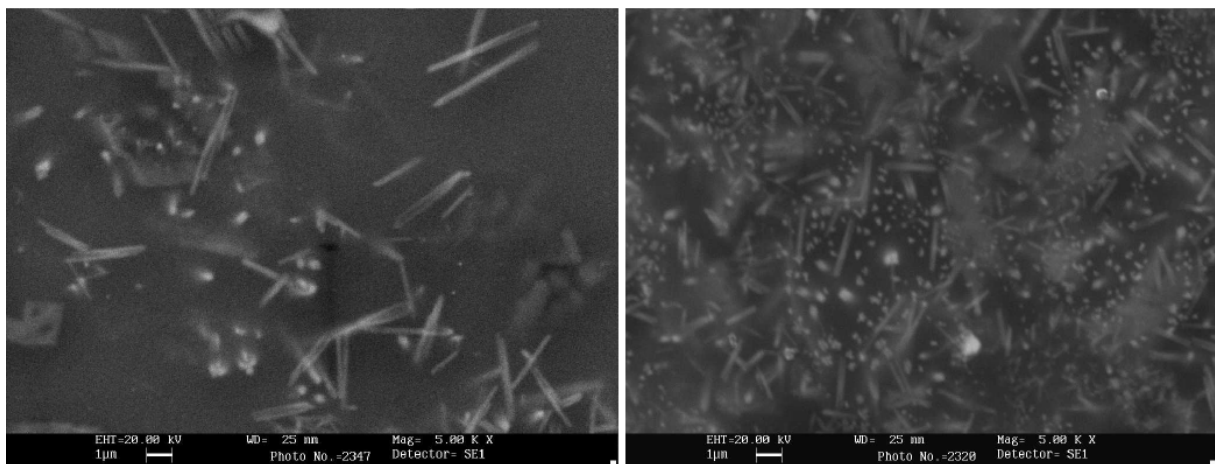


Figure 10. SEM photos of the glaze coatings obtained from 2.5%  $ZrO_2$  (left) and 12.5%  $ZrO_2$  (right) in the glaze composition.

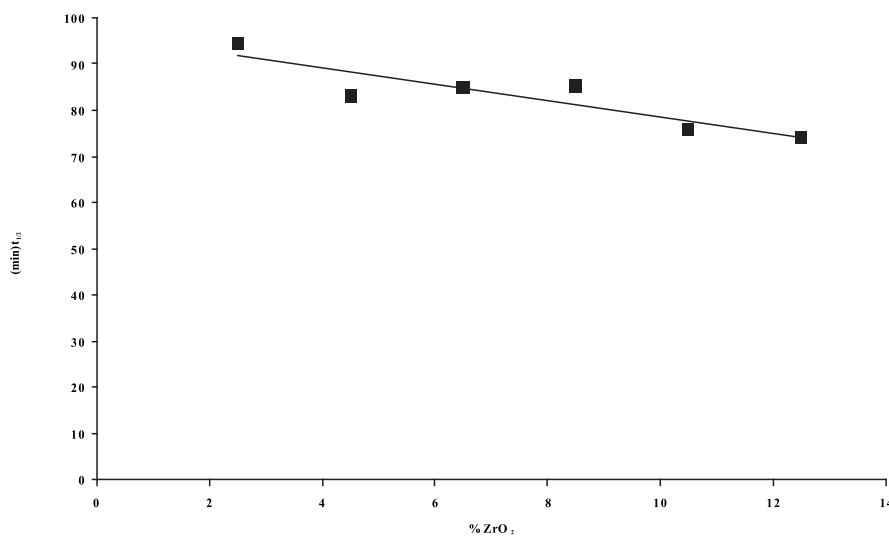


Figure 11. Variation of  $t_{1/2}$  with the  $ZrO_2$  % in the glaze.

In addition, the concentration of acicular crystals increases with the nominal quantity of  $ZrO_2$  in the composition. In accordance with this microstructure, surface gloss decreases gradually with the nominal quantity of  $ZrO_2$  in the composition while roughness increases. The greater quantity and smaller size of the Zircon crystals explain the improved photocatalytic activity with the increase in the nominal quantity of  $ZrO_2$  in the composition, while the measured half-life period decreases progressively in accordance with the Langmuir-Hinshelwood kinetic model (Figure 11). In short, the effect of crystal concentration and morphology is more determining than the band gap energy values.

#### 4.4. STUDY OF THE PHOTOCHEMICAL DEGRADABILITY OF ANATASE FILMS DEPOSITED ON CERAMIC GLAZES

Since the crystalline phase devitrification route did not lead to crystallisation of the  $TiO_2$  phase but to Titanite oxosilicate, and taking into account that, as is well known, Titanium lustres develop the Anatase phase, it was decided to study the photocatalytic degradability of these lustres.

For this study, layers with increasing  $TiO_2$  contents were deposited on the transparent standard porous single-fire glaze. This deposition was performed using the usual screen printing additives and vehicles employed in this type of application. The second firing was conducted at  $790^\circ C$ , yielding layers of lustres with different  $TiO_2$  contents. In order to confirm the crystallisation of Anatase, analysis was carried out by grazing incidence X-ray diffraction. Figure 12 presents the diffractograms corresponding to the different compositions. Anatase crystallisation begins to be noticed at 0.6%  $TiO_2$  and becomes quite evident at a concentration of 2.0%  $TiO_2$ .

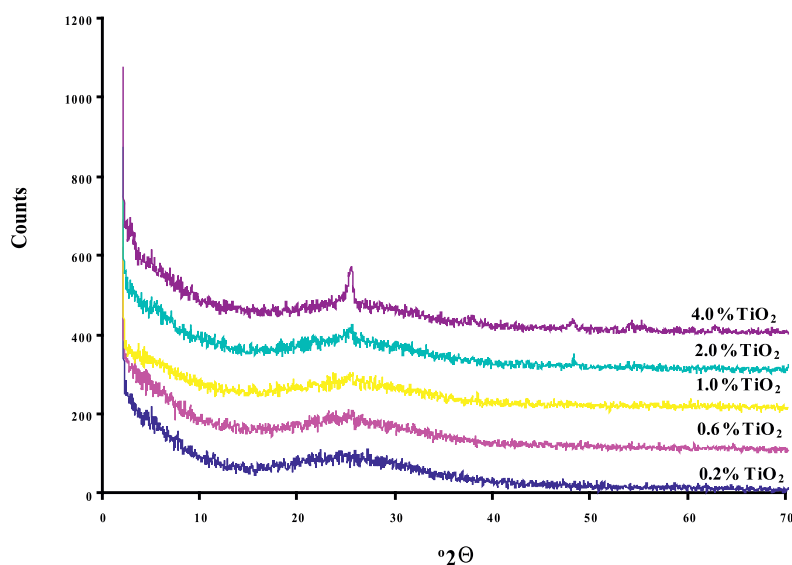


Figure 12. Grazing incidence X-ray diffraction of the layers of Ti lustre with different  $TiO_2$  contents.

These layers were then characterised, and the UV-V spectra were obtained (with which the  $E_g$  was calculated), in addition to the photocatalytic degradation curves. Figures 13 and 14 show the UV-V spectra and photocatalytic degradation, respectively, of the different layers.

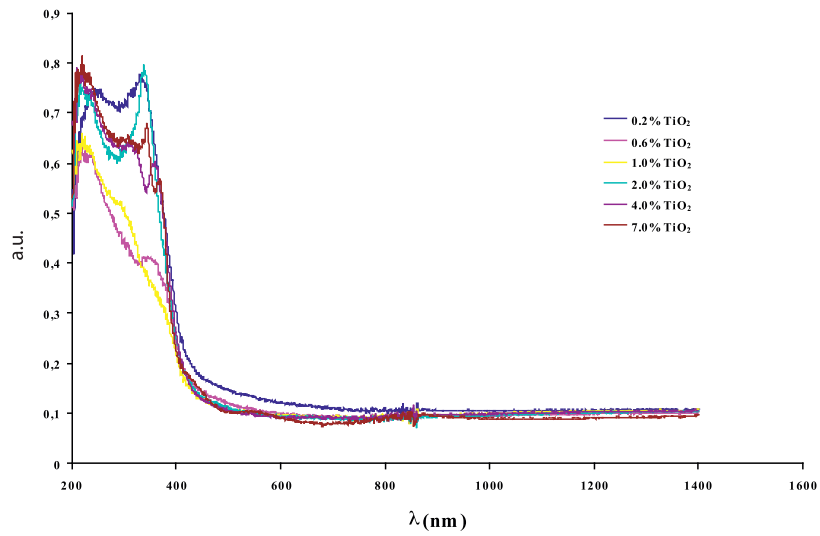


Figure 13. UV-V spectra of the glazes with Ti lustre.

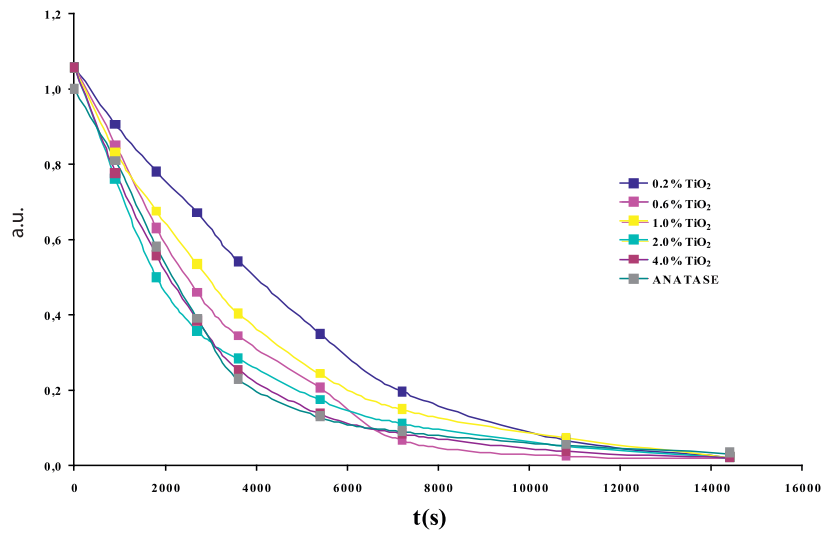


Figure 14. Evolution of the photocatalytic activity of the different Ti lustres and of the commercial Anatase.

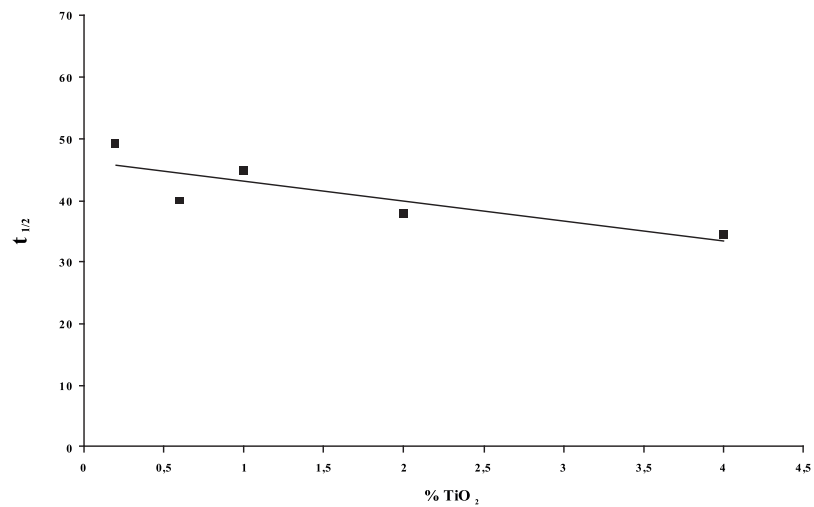


Figure 15. Evolution of  $t_{1/2}$  as a function of the  $\text{TiO}_2\%$  according to the Langmuir-Hinshelwood model.

Table 5 gives the values of  $E_g$  and  $t_{1/2}$  obtained for the different samples. The measured band gap energy lies around 2.9eV for the sample with 0.2%  $TiO_2$  and rises slightly with the increase to 4%  $TiO_2$ . In accordance with this energy value, the photocatalytic activity of the samples is excellent, as evidenced by the half-life periods obtained since they are similar or lower than the half-life period for the reference Anatase powder. In addition, the half-life period decreases progressively with the increase in  $TiO_2$  as Figure 15 shows, in which, following the Langmuir-Hinshelwood model kinetic, the Anatase percentage has been plotted against the half-life period.

% $TiO_2$	0.2	0.6	1.0	2.0	4.0
$E_g$ (eV)	2.89	2.90	2.90	3.03	3.03
$t_{1/2}$ (min)	49.3	40.0	44.8	37.9	34.5

Table 5. Values of  $E_g$  and  $t_{1/2}$  as a function of % $TiO_2$ .

## 5. CONCLUSIONS

1. The study has demonstrated the capacity of some glazes that devitrify certain crystalline phases to develop photocatalytic activity that degrades the Orange II organic colorant
2. Glazes with crystalline phases like Anorthite, Cassiterite and Zirconium Silicate improve photocatalytic degradability with respect to the initial standard transparent glaze.
3. When the devitrified Zirconium silicate content increased, the half-life period decreased and the photochemical degradability of Orange II therefore improved.
4. Although the band gap energy ( $E_g$ ) values in the glazes need to be low, this condition is necessary but not sufficient to develop glaze photocatalytic degradability.
5. The evolution of the microstructure plays an important role in the photocatalytic properties of a glaze because, for constant values of  $E_g$ , an increase in the concentration of the devitrified Zircon phase, as well as in crystal size, entails an improvement in the photocatalytic properties.
6. The optimum composition, from a photocatalytic viewpoint (minimum  $t_{1/2}$ ), of the Ti lustres corresponded to a  $TiO_2$  content of 4.0%.
7. The layers of Titanium lustre that crystallise Anatase develop a photocatalytic degradability equal to or greater than that of the Anatase powder, which evidences the potentiality of using glazes with Titanium lustre in discharge treatment processes.

## REFERENCES

- [1] Water Treatment Handbook Degrément. 6<sup>th</sup> Edition. Ed. Lavoisier Publishing, Paris (1991).  
 [2] O. Legrini, E. Oliveros, A.M. Braun, Chem. Rev., 93, 671-698 (1993).

- [3] C.P. Huang, Ch. Dong, Z. Tang, *Waste Management*, 13, 361-377 (1993).
- [4] US/EPA Handbook of Advanced Photochemical Oxidation Processes, EPA/625/R-98/004(1998).
- [5] S. Malato, M.I. Maldonado, J. Blanco, "Descontaminación de aguas de lavado de plaguicidas mediante fotocátalisis solar", CIEMAT, Spain, ISBN 84-7834-406-3 (2001).
- [6] Fallmann, H., Krutzler, T., Bauer, R., Malato, S., Blanco J., "Applicability of the Photo-Fenton method for treating water containing pesticides", *Catal. Today*, 54, pp. 309-319 (1999).
- [7] I.K. Konstantinou, T.A. Albanis, TiO<sub>2</sub>-assisted photocatalytic degradation of azo dyes in aqueous solution: kinetic and mechanistic investigations. A review, *App. Catalyst B: Environmental* 49(2004)1-14.
- [8] C. Hachem, F. Bocquillon, O. Zahraa, M. Bouchy, Decolourization of textile industry wastewater by the photocatalytic degradation process, *Dyes and Pigments* 49(2001)117-125.
- [9] Environmental photochemistry. Quantitative adsorption and FTIR studies during the TiO<sub>2</sub>-Photocatalyzed degradation of Orange II, *Langmuir* 16(2000)1102-1108.
- [10] R.P. Goehner, M.O. Eatough, A study of grazing incidence configurations and their effect on X-ray diffraction data, *Powder Diffraction* 7(1992)2-5.